Polarization Characteristics of Surface Plasmon Resonance in SnO2 Nanocluster Films

Article *in* Semiconductors · November 2011

DOI: 10.1134/S1063782611110108

CITATIONS
3

READS
29

8 authors, including:

Viktor Grinevich
Odessa National University
48 PUBLICATIONS **38** CITATIONS
SEE PROFILE

S. P. Rudenko
National Academy of Sciences of Ukraine
38 PUBLICATIONS **91** CITATIONS
SEE PROFILE

V. Smyntyna
Odessa National University
276 PUBLICATIONS **621** CITATIONS
SEE PROFILE

Liudmila Filevska
Odessa National University
37 PUBLICATIONS **33** CITATIONS
SEE PROFILE

ISSN 1063-7826, Semiconductors, 2011, Vol. 45, No. 11, pp. 1467–1473. © Pleiades Publishing, Ltd., 2011.
Original Russian Text © V.S. Grinevich, L.S. Maximenko, I.E. Matyash, O.N. Mischuk, S.P. Rudenko, B.K. Serdega, V.A. Smyntyna, L.N. Filevskaya, 2011, published in Fizika i Tekhnika Poluprovodnikov, 2011, Vol. 45, No. 11, pp. 1525–1532.

MICROCRYSTALLINE, NANOCRYSTALLINE, POROUS, AND COMPOSITE SEMICONDUCTORS

Polarization Characteristics of Surface Plasmon Resonance in SnO_2 Nanocluster Films

V. S. Grinevich[a]^, L. S. Maximenko[b], I. E. Matyash[b], O. N. Mischuk[b], S. P. Rudenko[b], B. K. Serdega[b], V. A. Smyntyna[a], and L. N. Filevskaya[a]

[a] *Mechnikov Odessa National University, ul. Dvoryanskaya 2, Odessa, 65082 Ukraine*

^*e-mail: grinevich@onu.edu.ua*

[b] *Lashkaryov Institute of Semiconductor Physics, National Academy of Sciences, pr. Nauki 41, Kyiv, 03028 Ukraine*

Submitted April 11, 2011; accepted for publication April 16, 2011

Abstract—Internal reflection features caused by the surface plasmon resonance in nanoscale films containing defect tin dioxide clusters in the stoichiometric dielectric matrix are studied by the method of polarization modulation of electromagnetic radiation. The angular and spectral characteristics of reflectances R_s^2 and R_p^2 of *s*- and *p*-polarized radiation and their polarization difference $\rho = R_s^2 - R_p^2$ are measured in the wavelength range $\lambda = 400–1600$ nm. The experimental characteristics $\rho(\theta, \lambda)$ (θ is the radiation incidence angle) obtained represent the optical property features associated with the film structure and morphology. Surface plasmon polaritons and local plasmons excited by *s*- and *p*-polarized radiation are detected; their frequency and relaxation properties are determined. The structural sensitivity of the technique for studying the surface plasmon resonance for tin dioxide films is shown.

DOI: 10.1134/S1063782611110108

1. INTRODUCTION

The urgency of developing and studying new nanoscale materials is caused by both fundamental interest in their properties and their potential applicability in solid-state electronics. The study of nanoscale tin oxide (SnO_2), in particular, is motivated by its numerous applications as transparent electrode materials, gas sensors, and catalysts in oxidation processes [1]. The list of applications of these nanostructures should also be complemented by the possibility of controlling light fluxes in materials in which surface plasmon resonance (SPR) effects are observed.

A working model of the object of this study (tin dioxide film) was constructed taking into account its surface specificity caused by dual Sn valence. Precisely this feature provides reversible transformations of the SnO_2 surface composition from stoichiometric Sn^{4+} to reduced Sn^{2+} depending on the chemical potential of oxygen of the system [1]. Surface reduction modifies its electronic structure and leads to the formation of deep electron levels in the band gap. This provides a decrease in the electron work function, the presence of free carriers in a material, and hence, the possibility of observing the SPR phenomenon.

Recently, a method for studying materials has become widespread, whose informative power is amplified by the properties SPR. It is generally believed that the SPR phenomenon is mostly characteristic of such metals as silver, gold, aluminum, and copper, whose permittivity becomes negative (the refractive index is less than unity) in the visible spectral region [2, 3]. This is the case if it is kept in mind that this phenomenon is observed by measuring the reflectance using one of the widespread optical schemes, i.e., the Otto [4] or Kretschmann geometry [5].

However, as shown recently [6], the SPR phenomenon can be observed even in the case when it is weakly detected from the viewpoint of conventional methods. The case in point is a relatively new method for measuring optically anisotropic effects, which is based on polarization modulation (PM) of electromagnetic radiation [7]. One version of this method yields a parameter called the polarization difference $\rho = R_s^2 - R_p^2$ of reflectances of radiation whose wave electric-field vectors are perpendicular and parallel to the incidence plane (optical axis), respectively. The increased detection and information powers of this parameter were multiply demonstrated in studying various effects of amplitude and phase anisotropy [6, 8].

It is well known that the reflection (including internal) phenomenon, under the conditions of which it is most convenient to measure the SPR, according to Fresnel formulas [9], heavily depends on the electromagnetic wave polarization state. These two factors stimulate application of the PM method to study nanoscale cluster films of tin dioxide. In contrast to nanoscale metal films, a feature of such objects is that their properties are controlled not only by the sample

Table

Sample type	*d*, nm	TDCDA content in the initial solution, %	PVA content in the initial solution, %
T4.R1	230–400	5	1
T4.R0.5	420	4	0.5
T2.R0.1	350	2	0.1
T2.R2	160	2	2
T0.5R0.1	80–100	0.5	0.1

surface state, but also by its bulk features. Therefore, it can be expected that the PM method will become an informative complement to such a widely used method of studying nanoscale objects as atomic-force microscopy.

The experience in using the PM method shows that it yields the polarization difference $\rho(\theta, \lambda, d, ...)$ parameters (θ, λ, and d are the incidence angle of light, wavelength, and film thickness, respectively, etc.), which are multivalued and multivariant in form. They contain information on both the optical properties of objects under study and their morphology and structure.

In this case, special attention should be paid to certain advantages in using films consisting of particles that are isolated or contacting with each other in comparison with continuous films. In particular, the prohibition associated with the difference of wave vectors during the interaction of light and plasmon excitation in films is cancelled for particles due to the presence of surface curvature [10]. Furthermore, this prohibition, as we have shown previously [8], is also lifted for the initial state of radiation polarization in the sense that not only *p*-polarized, but also *s*-polarized radiation with respect to the incidence plane excites SPR in the cluster film.

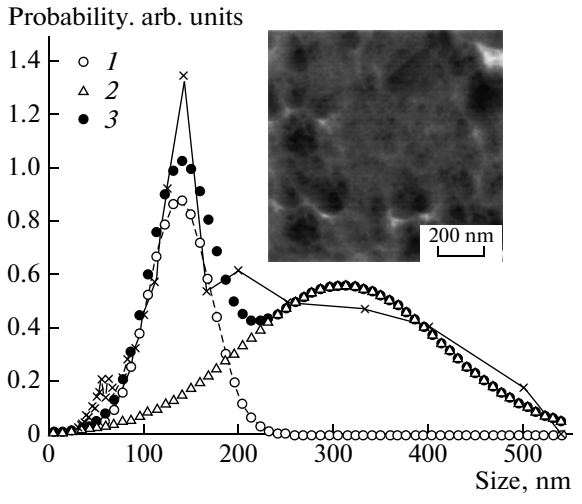

Fig. 1. Histogram of the probabilistic-size composition of sample T4.R1: the Fourier spectrum of the surface profile (solid curve) (*1*, *2*) expanded in Gaussian curves and (*3*) their sum. The inset shows the AFM phase topology.

There are known SPR studies in nanocomposite films representing Al, Au, and ITO metal clusters in the dielectric matrix of WO_3, SnO_2, and TiO_2 oxide materials [11]. In this study, nanostructured tin oxide films are considered as nanocomposite ones representing clusters of defect nonstoichiometric tin oxide (SnO_x) in the dielectric matrix of stoichiometric SnO_2. Thus, object of this study is to interpret their properties based on experimental data on SPR obtained by the polarization modulation technique.

2. EXPERIMENTAL

Samples were prepared by the technique described in detail in [12]. This technique contained the following basic stages: preparation of an acetone solution of the polymer (PVA), preparation of an acetone solution of the SnO_2 precursor, mixing of these two solutions, applying on a substrate by the rotational method using centrifuging (spin-coating), drying, and annealing. As a tin dioxide precursor, tin dichlorodiacetylacetonate (TDCDA) complex was used. A cover glass 22 × 22 mm was used as a substrate. Samples were kept at room temperature for 15 min to remove acetone and were then annealed in air at 600°C for 6 h for thermal decomposition of organic components (TDCDA and PVA) and removal of their decay products. After annealing, tin dioxide formed by TDCDA thermal decomposition remained on the substrate, which was shown in studies of properties of this precursor [13]. PVA was used to structurize the film at the stage of solution preparation and applyication on the substrate.

The main sample parameters are listed in the table. The data on the film thickness averaged over the studied area surface (1 × 1 μm) were measured by atomic-force microscopy (AFM) with an error no more than 2% in the indicated range.

The inset to Fig. 1 shows the phase topology of the 1000 × 1000 nm surface of sample T4.R1, obtained using a commercial Nanoscope IIIa (Digital Instruments, USA) atomic-force microscope. The histogram of the probabilistic-size film composition, obtained using Fourier expansion of the surface profile, is shown in Fig. 1 by the solid curve. Histograms approximated by Gaussian functions show that the film consists of two groups of clusters commensurate in histogram areas. One of them spans sizes in the range of 50–200 nm with an extremum at 137 nm; the one with an extremum at 310 nm occupies the range of 200–500 nm. Note that comparison of the visual evaluation of the film with its presented quantitative characteristic allows the conclusion that large clusters are isolated conglomerates consisting of smaller clusters separated by nanoscale spacings of thermal origin. As will be shown below, this feature of the film has an effect on the shape of its spectral characteristics. The

identified cluster structure of the film with a large number of defects (the crystallite–cluster interfaces) promotes the formation of electron plasma in the films under study.

The samples were arranged on the reflecting surface of a total internal reflection semicylinder made of fused silica whose refractive index $n = 1.45$ defined the critical angle $\theta_{cr} = 42°$. The radiation source was a system consisting of an incandescent lamp and a monochromator with an Ahrens prism at the output slit. The internal reflectances R_s^2 and R_p^2 of radiation polarized perpendicular and parallel (*s*- and *p*-polarization, respectively) with respect to the light incidence plane and their polarization difference $\rho = R_s^2 = R_p^2$ were measured depending on the light incidence angle in one case and on the wavelength in the range of $\lambda =$ 400–1600 nm in the other case. Their measurements performed using PM are described in detail in [6]. Here, we briefly note that the role of modulation in this study consisted in alternate irradiation of our sample with *s*- and *p*-polarized radiation without changing the electromagnetic wave intensity. In this case, the modulation frequency was so low (50 kHz) that itdid not affect the electromagnetic wave frequency.

The polarization modulator was placed in front of the sample and, functioning in the quarter-wave phase plate mode, transformed circularly polarized radiation from the steady state to a periodically varying linear one. Wave field azimuths were oriented parallel and perpendicular to the semicylinder axis. In this case, the value measured at the modulation frequency is the polarization difference of *s*- and *p*-functions whose arguments in this case are the wavelength (energy) and light reflection angle. The appropriateness of the used technique consists in the fact that the result is the physical difference of two terms. Therefore, it becomes reliable even when the difference signal is lower than the noise of either term. It is especially important in the case of the long-term instability that, as a rule, accompanies independent measurements of dependences. Furthermore, the physical (in this case) subtraction of experimental functions makes it possible to increase the measurement reliability by amplifying insignificant differences due to "zeroing" (subtraction of general features).

The addition of the linear polarizer to the optical scheme allowed the use of the latter for measuring the reflectances R_p^2 and R_s^2. To this end, the polarizer was placed behind the modulator so that its axis would coincide, in one case, with the semicylinder axis, and would be perpendicular to it in the other case. The polarizer played the role of the window that was adjusted by rotation to transmission of correspondingly polarized radiation, thus ensuring an alternating signal at the photodetector during modulator operation. *s*- or *p*-polarization controlled by the linear polarizer azimuth was identified by the ratio of signals measured for radiation reflection from a semicylinder with a clean reflecting surface; in the entire range of angles smaller than the critical, $\theta < \theta_{cr}$, according to the Fresnel formulas, this radiation satisfies the condition $R_s^2 > R_p^2$.

It is noteworthy that the measured reflectances refer to the radiation intensity, and their magnitudes are always positive. However, this does not concern parameter ρ, which, depending on the relation of its terms, can be negative, $\rho < 0$. As will be shown below, this takes place in the case of "anomalous" reflection at $R_s^2 < R_p^2$, which appears in some cases in the range of angles larger than the critical one θ_{cr}. Since measurements were performed using a phase-sensitive (lock-in) nanovoltmeter, the sign of parameter ρ was calibrated by the relation $R_s^2 > R_p^2$ obtained by reflection from the clean semicylinder surface. This procedure is carried out by setting the corresponding phase of the reference signal in the indicated measuring device; this value is the alternating supply voltage of the polarization modulator.

3. RESULTS AND DISCUSSION

We will discuss the results from the position of Fresnel formulas in the form of an equation describing the dependences of the reflectances R_s^2 and R_p^2, hence, the dependence of the polarization difference ρ on the light incidence angle θ. This equation is given in [6]; it was obtained by the method of matrix transformation of Fresnel formulas for the three-layer glass–film–air model, in which the cluster film is considered to be planar and homogeneous one with effective optical parameters. This approach is based primarily on the results of AFM studies, which showed that the film surface is smooth with roughness insignificant relative to the thickness. At the same time, taking into account such a sample feature as a structural heterogeneity and the incommensurability of clusters and the wavelengths used, we believe that the characterization of sample dielectric properties by effective optical parameters is quite adequate.

The experimental results, i.e., the dependences of the reflectances R_s^2 and R_p^2 and their polarization difference ρ on the radiation incidence angle, are shown in Fig. 2 for sample T4.R1 in comparison with the calculation result. The reason for the choice of the wavelength $\lambda = 500$ nm will be understood from further discussion; for now, we recall that the characteristic feature of the SPR in metal homogeneous films of optimum thickness is, by definition, the dip in the function $R_p^2(\theta)$, narrow in angular coordinate and deep in amplitude.

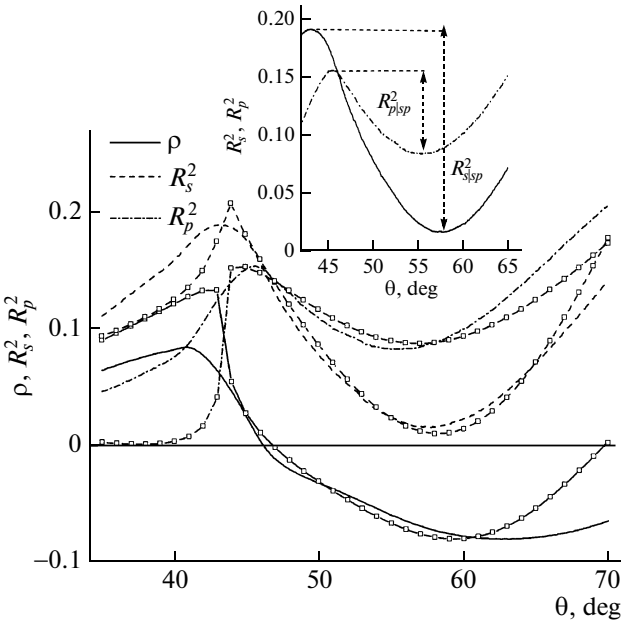

Fig. 2. Experimental (curves) angular dependences of the internal reflectances $R_s^2(\theta)$, $R_p^2(\theta)$ and the parameter $\rho(\theta)$ in sample T4.R1 in comparison with calculated (dots) characteristics. The calculation is performed for the following parameters: $\lambda = 500$ nm, $n = 1.61$, $k = 0.1$, $d_p = 290$ nm, and $d_s = 300$ nm. The inset shows the different degrees of resonant interaction characterized by the values of $R_{s|sp}^2$ and $R_{p|sp}^2$ in sample T4.R1.

We can see in Fig. 2 that the characteristic features of SPR take place not only in $R_p^2(\theta)$, but also in the $R_s^2(\theta)$ curve, which, in the angular range above the critical one, $\theta > \theta_{cr} = 42°$, contains the indicated reflectance slope. The fact that this slope is more extended in comparison with the similar characteristic of metal films uniform in thickness does not contradict the nature of the appearance of the SPR phenomenon in spherical or close-to-spherical objects [10]. The reason is that the light incidence angle in the case under consideration should be measured not from the film surface, but from the plane tangent to the cluster surface, hence, arranged at a certain angle to the film plane.

The refractive indices (n) and absorbances (k) of tin dioxide cluster films in dielectrics necessary to calculate the coefficients R_s^2, R_p^2, and the parameter ρ were determined from the condition of coincidence of calculated and experimental results, which is attained by multiparametric fitting. Agreement of these data was achieved using a certain artificial approach, i.e., the use of modified Fresnel formulas in the equation given in [6]. The physical nature of the modification is based on the fact that an s-polarized wave for the cluster film (in contrast to a homogeneous one) contains a field component oriented in the general case along the normal to the cluster surface. This is formally considered in the form of different sample thicknesses (d_s, d_p) in the wave field directions with orthogonal azimuths. The applicability of such an approximation does not contradict the shape anisotropy concept discussed in [9]. Apparently, an increase in the number of fitting parameters by adding one more unknown complicates the matching process. However, experience has shown that the variation range of parameters was limited to several decimal places. Therefore, because the film thickness was known, fitting by selection of refractive indices and absorbances in a limited range was not complicated.

The determined values of the optical constants are in logical agreement with the data of [14]. As to the observed disagreement in angular dependences, it should be noted that the film is slightly wedge-shaped and is inhomogeneous within the light spot, whose size increases with angle. Furthermore, in the general case, the geometrical shape of clusters is not spherical, which would be reflected by an additional condition. Nevertheless, the observed agreement of calculated and measured data in Fig. 2 is more than satisfactory.

Furthermore, at first glance, an unusual conclusion follows from Fig. 2: the SPR phenomenon in metal–dielectric cluster films can also be detected in the case of surface plasmon excitation by unpolarized radiation. It is easy to verify that the above-mentioned shape of clusters leads to resonant interaction of radiation with their electron system not only for p-polarized radiation, as in the case of continuous homogeneous metal films, but also for s-polarization. Moreover, if we take into account that the amplitudes of the extrema of corresponding polarization branches reflect the intensities of the resonant interaction, it follows from the inequality of the reflectances in the resonance region, $R_{s|sp}^2 > R_{p|sp}^2$ (inset to Fig. 2), that the shape of clusters and/or their dielectric stoichiometric environment is more preferable according to the conditions of the appearance of SPR for s-polarization. This condition is the relation called the phase matching condition [3],

$$\sqrt{\varepsilon_0}\sin\theta_{sp} = \sqrt{\frac{\varepsilon_2\varepsilon_1(\omega)}{\varepsilon_2 + \varepsilon_1(\omega)}} \qquad (1)$$

following from the equality of wave vectors of excitation and plasmon waves. Here ε_0, $\varepsilon_1(\omega)$, and ε_2 are the real parts of the complex permittivities of the prism, metal film, and external medium materials, respectively. Equation (1) expresses the equality of the projection of the wave vector $\mathbf{k}_0$ (left-hand side) of radiation propagating in the prism at the resonance angle θ_{sp} on the metal film and the vector $\mathbf{k}_{sp}$ of the plasmon wave propagating along the surface. The validity of the involvement of known relation (1) is that one of its parameters, i.e., θ_{sp}, being an argument of the function

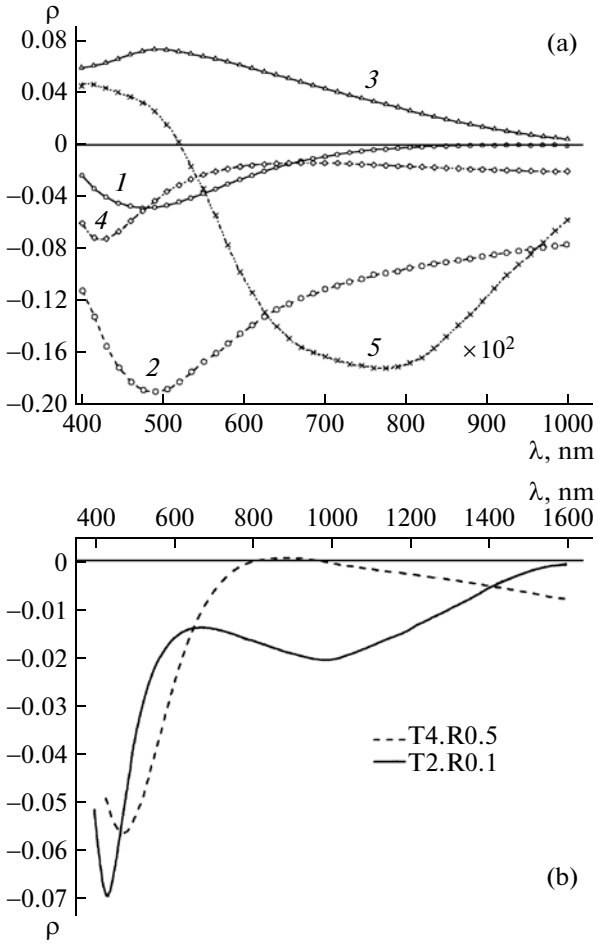

Fig. 3. Spectral dependences of the polarization difference ρ(λ) at an angle of incidence of 55°: (a) samples (*1*) T4.R0.5, (*2*) T4.R1, (*3*) T0.5.R0.1, (*4*) T2.R0.1, and (*5*) T2.R2; (b) samples T4.R1 and T4.R0.5, extended wavelength range.

ρ(θ), illustrates the possibility of exciting a surface plasmon wave in a wide angular range due to the nonplanar cluster surface.

The resonant interaction is also suggested by the spectral characteristics of the parameter ρ(λ) (see Fig. 3) for samples differing in tin dioxide thickness and content. Here, the actual sign of parameter ρ is retained everywhere; in particular, for three dependences, the negative sign of the relation $\rho = R_s^2 - R_p^2$ relates to actually measured quantities. From Fig. 3a, the reason becomes clear for the choice of the wavelength for the angular dependence of parameter ρ(θ), shown in Fig. 2 for sample T4.R1. We can see that the curves ρ(λ) in the wavelength range λ = 400–500 nm contain an extremum for all samples. In this case, the negative sign of characteristics indicates satisfying the relation $R_s^2 < R_p^2$, hence, surface plasmon excitation by *s*- and *p*-polarized radiation, which is consistent with the

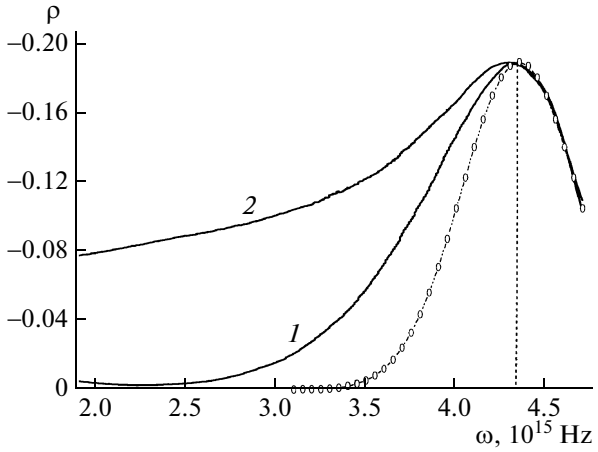

Fig. 4. Frequency dependences of parameter ρ of samples (*1*) T4.R0.5 and (*2*) T4.R1, recalculated from the data of Fig. 3a and normalized to the extremum, in comparison with the normal Gaussian distribution function (dots).

angular dependences (Fig. 2) of both R_s^2 and R_p^2 and their polarization difference.

Moreover, the value and sign of the parameter ρ and the positions of extrema of curves have a certain correlation with the sample thickness and the SnO_2 precursor content in initial solutions. Comparison of sample parameters with the value and sign of the polarization difference ρ shows that an increase in the SnO_2 precursor content results in a decrease in parameter ρ amplitude along the vertical axis. It is noteworthy that the data for sample T2.R2, consistent with the observed trend, are scaled up to avoid merging of the characteristic with the horizontal axis. The correlation between the precursor content and the resonant frequency is qualitatively consistent with the tendency according to which the frequency increases with the material conductivity.

The existence of resonant interaction of another nature in the studied films is suggested by Fig. 3b, which shows the spectral curves ρ(λ) for two samples in the extended wavelength range. One of them has an extremum at λ ≈ 950 nm typical of the resonance effect; another, due to the limited range, exhibits a trend toward an increase, which without a doubt should lead to an extremum. The nature of these extrema will be identified by the corresponding spectral analysis.

Figure 4 shows two curves ρ(λ) from Fig. 3 for samples T4.R0.5 and T4.R1, recalculated to the frequency dependences ρ(ω), i.e., to the form conventional for imaging resonant phenomena. Furthermore, for clarity, they are reduced to the same amplitude of the extremum. We can see the identity of both characteristics to the right from the resonant frequency $\omega_0 = 4.3 \times 10^{15}$ Hz, which indicates the general nature of the phenomenon in this frequency range. Since the

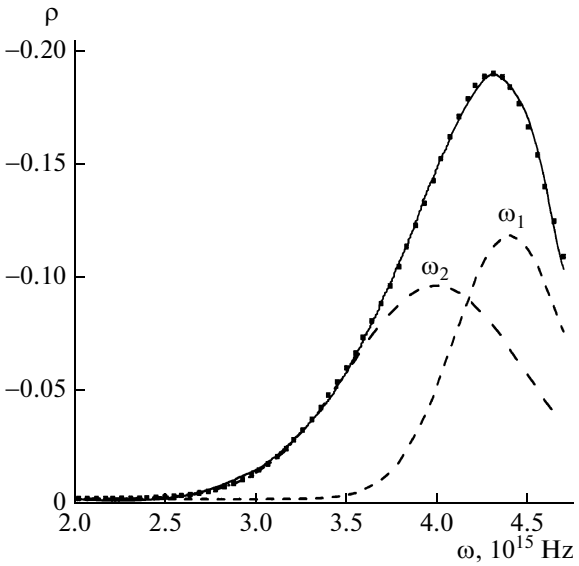

Fig. 5. Frequency dependence of the parameter ρ of sample T4.R0.5 (dots), recalculated from the corresponding dependence ρ(λ) (Fig. 3a) in comparison with the normal Gaussian distribution function (solid curve) expanded in two components (dashed curves).

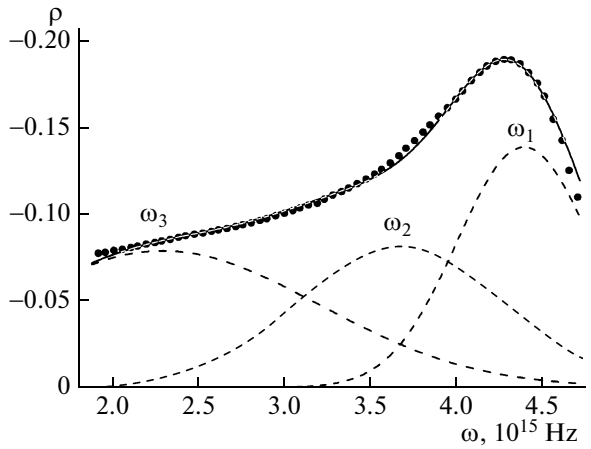

Fig. 6. Frequency dependence of parameter ρ for sample T4.R1 (dots), recalculated from the corresponding dependence ρ(λ) (Fig. 3a) in comparison with the Gaussian distribution function (solid curve) expanded in three components (dashed curves).

samples were prepared with the same amount of the tin dioxide precursor, it is reasonable to relate the identity of resonant frequencies to identical number of centers interacting with the wave. Since this range is near the flattening region of the dispersion dependence $\omega(k)$ describing the resonance phenomenon, we can conclude that the nature of this extremum is associated with the local plasmon resonance at cluster particles.

However, curves *1* and *2* in Fig. 4 are more complex than the elementary oscillator function, which is suggested by the obvious asymmetry of the curves with respect to the resonant frequency ω_0 and, as a result, by their disagreement with the normal distribution function (dots) in the range of frequencies lower than ω_0. These circumstances necessitated the approximation of the former by two Gaussian functions, the result of which is shown in Fig. 5. We can see that the approximation is so ideal that it allowed the determination of the key resonance parameters, i.e., the frequencies (ω_1, ω_2) and relaxation times (γ_1, γ_2). It is reasonable to relate this result in the form of two components of the parameter $\rho(\omega)$ to two groups of clusters differing by sizes, shown in Fig. 1. Supposing that the relaxation time of the local plasmon energy is controlled by scattering at the surface, it is reasonable to attribute the parameters $\omega_1 = 4.4 \times 10^{15}\ s^{-1}$, $\gamma_1 = 1.67 \times 10^{-13}$ s and $\omega_2 = 4 \times 10^{15}\ s^{-1}$, $\gamma_2 = 1.02 \times 10^{-13}$ s to clusters with increased and decreased sizes, respectively.

The same procedure was efficiently applied to the second, more complex dependence of Fig. 4. In sample T4.R1, in addition to two components typical of sample T4.R0.5, there exists one more resonant electromagnetic interaction in the frequency range under study, i.e., excitation of the plasmon–polariton wave in the film, caused by the intercluster dipole–dipole interaction [15]. This interaction is illustrated in Fig. 6 by an additional component which, being summed with two other Gaussian curves (the sum is the solid curve), is in good agreement with the experimental dependence (dots). The conditions of its appearance and the degree of its manifestation depend, in contrast to the local surface resonance, not only on the total number of interacting centers, but also on sizes, shape of clusters, and the distance between them, which has suggested by, e.g., [16].

This fact is directly confirmed by the surface plasmon–polariton wave excitation, which is reflected in the formation of a resonant extremum of the spectral characteristics of the parameter $\rho(\omega)$ for sample T2.R0.1 (Fig. 3b) near the wavelength $\lambda = 980$ nm and in the tendency of the curve for sample T4.R0.5, which should lead to a resonant extremum with high probability. Exactly this resonance, which is spaced at a fairly long distance from the local one in samples T4.R0.5 and T2.R0.1, coming closer to local resonances in frequency (ω_1 and ω_2 in Fig. 6) in sample T4.R1, increases the amplitude of the corresponding curve in Fig. 3a.

Detailed reasons for the appearance of the above features in the spectral characteristics can be the subject of an independent study. Identification of the reasons can be facilitated by data on the parameters of local and polariton resonances. Such data are the resonant frequencies $\omega_1 = 4.38 \times 10^{15}$, $\omega_2 = 3.67 \times 10^{15}$, $\omega_3 = 2.3 \times 10^{15}$ Hz and the oscillation relaxation times $\gamma_1 = 1 \times 10^{-15}$, $\gamma_2 = 0.71 \times 10^{-15}$, $\gamma_3 = 0.48 \times 10^{-15}$ s

obtained for three components from the Gaussian functions (Fig. 6).

4. CONCLUSIONS

The general principles of the occurrence of the SPR phenomenon [3] do not exclude the possibility of its observation in tin dioxide films. Nevertheless, except for the small-scale study [17], to our knowledge, there are no publications with detailed results of its observation. The appropriateness of studies in this line is dictated not only by the circumstances noted in the Introduction, but also by the observed strong response of the parameter ρ to changes in both a film's optical properties and external medium parameters. Therefore, it seems promising to use these properties not only in sensor applications, but also in physical problems of the near field. However, solving these problems requires corresponding technological support and fabrication of films with controllable and reproducible parameters.

As for the problem posed in this study, in particular, it is shown that the negative sign of the polarization difference (anomalous reflection) $\rho = R_s^2 - R_p^2$ points to the metal nature of absorption in films. However, as we have shown previously [8], the range of negative ρ and the shape of its angular dependence differ significantly for continuous and cluster films. For example, its increased extension in the range of angles larger than the critical one is exclusively associated with the material cluster structure. This fact, confirmed by independent studies, can be a basis for its application as a diagnostic tool. Furthermore, with reasonable justification, the results obtained make it possible to solve the most important problem of composite nanomaterials, i.e., determination of the cluster shape. Information on the latter can be obtained from the relations of $R_{s|sp}^2$ and $R_{p|sp}^2$, characterizing the degree of resonant interaction, and the angular and spectral dependences of the parameter ρ. The used spectral analysis technique makes it possible to obtain information on the nature of resonances, their frequency and relaxation parameters, and the related structural and crystalline perfection of samples.

ACKNOWLEDGMENTS

We are grateful to Prof. Byulent Ulug and researchers of the Solid State Physics Department of Akdeniz University (Antalya, Turkey) for assistance in sample preparation, and to Oksana Litvin (Lashkaryov Institute of Semiconductor Physics) for her assistance in atomic-force microscopy studies.

REFERENCES

1. M. Batzill and U. Diebold, Progr. Surf. Sci. **79**, 47 (2005).
2. *Surface Polaritons. Electromagnetic Waves at Surfaces and Interfaces* Ed. by V. M. Agranovich and D. L. Mills (North Holland, Amsterdam 1982; Nauka, Moscow, 1985).
3. N. L. Dmitruk, V. G. Litovchenko, and V. L. Strizhevskii, *Surface Polaritons in Semiconductors and Dielectrics* (Nauk. dumka, Kiev, 1989) [in Russian].
4. A. Z. Otto, Z. Phys. **216**, 398 (1968).
5. E. Z. Kretschman, Z. Phys. **241**, 313 (1971).
6. L. I. Berezhinskii, L. S. Maksimenko, I. E. Matyash, S. P. Rudenko, and B. K. Serdega, Opt. Spectrosc. **105**, 257 (2008).
7. S. N. Jasperson and S. E. Schnatterly, Rev. Sci. Instrum. **40**, 761 (1969).
8. L. I. Berezhinskii, O. S. Litvin, L. S. Maksimenko, I. E. Matyash, S. P. Rudenko, and B. K. Serdega, Opt. Spectrosc. **107**, 264 (2009).
9. M. Born and E. Wolf, *Principles of Optics* (Cambridge Univ. Press, Cambridge, 1999).
10. E. A. Vinogradov, E. A. Leskova, and A. P. Ryabov, Opt. Spectrosc. **76**, 282 (1994).
11. Sarika Singh and B. D. Gupta, Meas. Sci. Technol. **21**, 115202 (2010).
12. L. N. Filevskaya, V. A. Smyntyna, and V. S. Grinevich, Photoelectronics (Odessa) **15**, 11 (2006).
13. B. Ulug, H. M. Türkdemir, A. Ulug, O. Büyükgüngör, M. B. Yücel, V. S. Grinevich, L. N. Filevskaya, and V. A. Smyntyna, Ukr. Chem. J. **7**, 12 (2010).
14. M. Anastasescu, M. Gartner, S. Mihaiu, C. Anastasescu, M. Purica, E. Manea, and M. Zaharescu, in *Proceedings of the IEEE International Semiconductor Conference* (2006), vol. 1, p. 163.
15. A. B. Yevlukhin, JTP Lett. **31**, 14 (2005).
16. A. S. Shalin and S. G. Moiseev, Opt. Spectrosc. **106**, 916 (2009).
17. B. K. Serdega, I. E. Matyash, L. S. Maximenko, S. P. Rudenko, V. A. Smyntyna, V. S. Grinevich, L. N. Filevskaya, B. Ulug, A. Ulug, and B. M. Yucel, Semiconductors **45**, 316 (2011).

Translated by A. Kazantsev